Electrically controlled quantum reflection

A. Ronny Barnea,[1] Benjamin A. Stickler,[2] Ori Cheshnovsky,[1] Klaus Hornberger,[2] and Uzi Even[1]
[1]*School of Chemistry, Sackler Faculty of Exact Sciences, Tel Aviv University, Tel Aviv 69978, Israel*
[2]*Faculty of Physics, University of Duisburg-Essen, Lotharstraße 1, 47048 Duisburg, Germany*
(Received 6 February 2017; published 27 April 2017)

We demonstrate experimentally that an electric field can be used to control quantum reflection of matter waves off periodically microstructured surfaces. Applying a voltage of alternating polarity between neighboring grating bars induces an electric field which modifies the interaction between the surface and the impinging matter wave so that quantum reflection is gradually reduced. We find that the measured reflectivities are in good agreement with our numerical simulations and that their suppression is well captured by a simple analytic model. This experiment constitutes a step towards electrically tuned reflective diffraction elements for atomic and molecular matter waves.

DOI: 10.1103/PhysRevA.95.043639

I. INTRODUCTION

Quantum reflection, the classically impossible reflection of a particle in the absence of a turning point [1], has attracted considerable attention over the last decades. First observed through the reduction of sticking coefficients [2–5], reflection off the attractive tail of the atom-surface interaction potential was studied for various systems, such as hydrogen atoms reflected off a thin film of liquid helium [6–8], metastable neon atoms scattered from solid surfaces [9–11], helium atoms reflected off an α-quartz crystal [12] or a rough surface [13], and Bose-Einstein condensates reflected off a wall [14–16]. The use of periodically microstructured gratings enabled the observation of quantum reflection into multiple diffraction orders [17–20]. The fact that such diffraction gratings are mass selective and that quantum reflection occurs far away from the surface makes them attractive for atomic and molecular metrology, in particular with weakly bound species [18].

Quantum reflection gratings join in to a number of other coherent manipulation techniques for atomic and molecular matter waves such as transmissive diffraction gratings [21–23], Poisson spot plates [24,25], ridged mirrors [11,26,27], and Fresnel zone plates [28,29]. The operation of these matter-wave optical elements depends crucially on the interaction between their surface and the impinging particle [30,31].

In most quantum reflection experiments, the interaction between the surface and the incident matter wave is well described by the Casimir-Polder potential [32,33]. Thus, the semiclassical Wentzel-Kramers-Brillouin (WKB) waves well approximate the exact wave function both near and far from the surface [34–36]. This allows one to identify regions which strongly contribute to the reflectivity, referred to as the *badlands* [36–38], and to explain why quantum reflection typically occurs tens of nanometers above the surface [13,18,36]. For slowly approaching particles one finds that the reflectivity off the Casimir-Polder potential decreases exponentially with increasing incident velocity [36].

Here, we report on the controlled suppression of quantum reflection, using a conductive bipolar electrical grating deposited on the oxide layer of a grounded silicon surface. Applying a static voltage of alternating polarity between neighboring grating bars produces an electric field which can suppress quantum reflection [39]. We measure the reflectivity as a function of the applied voltage and find good agreement with the theoretical prediction. Our findings are also well explained by an approximate model which attributes the reduced reflection probability to the increase in kinetic energy due to the electric field. The latter increases the impact velocity of the matter wave in a controlled fashion so that the quantum reflection probability off the Casimir-Polder potential can be tuned. This experiment constitutes a step towards the realization of more complex electrically tunable matter-wave reflection devices.

We start by introducing our experimental setup and the electric-field-induced interaction potential between the surface and the matter wave. The experimentally observed reflectivities are then compared to numerical simulations and to an analytic model, developed to understand qualitatively the reduction of reflectivity with increasing bias.

II. EXPERIMENTAL SETUP

The beam system is schematically shown in Fig. 1: A helium beam is generated in the source chamber by a cryogenically cooled Even-Lavie pulsed valve [40]. The beam transits an ultrahigh-vacuum collimation chamber and enters the interaction chamber, where its final angular width is set before it approaches the reflection grating at grazing incidence. The specularly reflected part of the beam is detected by a time-of-flight mass spectrometer [41] (see Appendix A).

The Even-Lavie valve is operated at 35 K with helium at a pressure of 2 bar and yields a beam with velocity $v = 605 \pm 5$ m/s. Initial collimation of the beam is achieved by two custom tilted-razorblade skimmers with an opening of 150 μm, positioned 475 and 745 mm downstream from the source. An additional 100-μm movable slit positioned 115 mm after the second skimmer sets the angular dispersion of the beam to 250 μrad (half width at half maximum). The beam approaches the reflection grating, which is positioned 60 mm ahead of the slit, at an incidence angle of roughly $\theta \simeq 1$ mrad. The grating is mounted on a linear and rotational nanopositioning piezomotor assembly.

The small incidence angle $\theta \simeq 1$ mrad defines the velocity component perpendicular to the surface, $v_y = v \sin\theta \simeq$

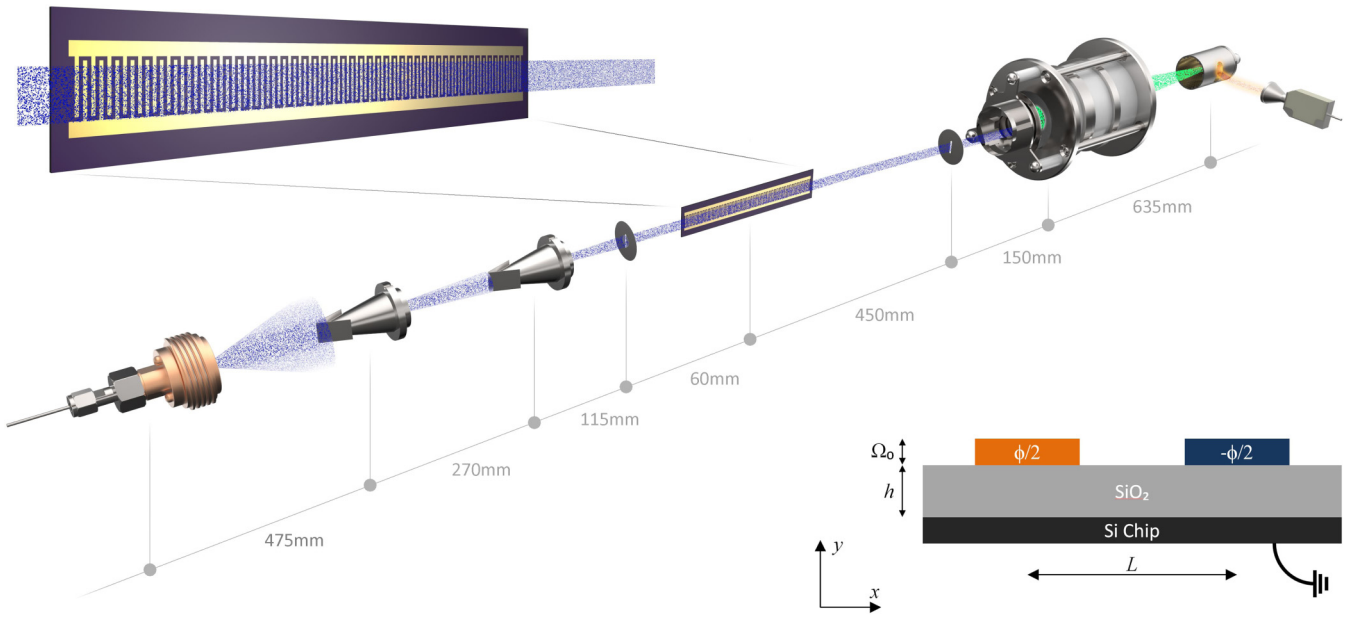

FIG. 1. Overview of the beam system used in the experiment. A collimated helium beam with velocity $v = (605 \pm 5)$ m/s is quantum reflected off the grating and subsequently detected using a time-of-flight mass spectrometer. The grating, consisting of thin conductive bars of period $L = 10$ μm, is fabricated on a SiO_2 dielectric layer of thickness $h = 1$ μm. The grating bars of height $\Omega_0 = 30$ nm are biased alternatingly at voltages $\pm\phi/2$.

0.6 m/s, which is comparable to previous quantum reflection experiments with helium [13]. The grating was fabricated using standard photolithography methods. It consists of 4500 interdigitated metallic grating bars of 3 mm length, 5 μm width, and period $L = 10$ μm, which can be biased at voltages of alternating polarity (see inset in Fig. 1). The substrate is highly doped p-type silicon covered with a thermal oxide layer of thickness $h = 1$ μm. The grating bars on top of the polished oxide layer consist of a 25-nm gold layer above 5 nm of chromium ($\Omega_0 = 30$ nm). The silicon substrate is grounded. The maximum bias voltage between adjacent grating bars was limited to 160 V to avoid arcing or significant leakage.

The reflected part of the helium beam is selected by a 200-μm-wide scanning slit mounted on a linear nanopositioning stage, movable perpendicular to the beam axis, 450 mm away from the grating. The selected part of the beam is ionized by electron impact before entering a time-of-flight mass spectrometer [41]. The ions are then detected with an efficiency close to unity by a large-area secondary electron dynode and a channel electron multiplier [42].

III. ALIGNMENT AND LIMITATIONS

The grating was aligned with respect to the signal of the direct (unreflected) beam, by translating it into and out of it, and rotating it around its axis, perpendicular to the plane of the beam [43]. To measure the specular reflection probability, the grating was rotated to $\theta \simeq 1$ mrad and then translated such that it yielded the maximum signal with the detection slit selecting the signal at an angle of 2 ± 0.2 mrad. We estimate the accuracy of the grating rotation to be about 100 μrad. Some vibrations were inherent in the experimental setup (mainly due to the cryogenic cooling mechanism) and might have generated some further error. Oscillations of up to 100 μrad were recorded in the encoder of the nanopositioning rotation stage while the system was running, and as such the error in the incidence angle is taken to be $\Delta\theta \simeq 150$ μrad. In addition, the angular dispersion of the beam translates into an uncertainty of ± 0.15 m/s in the velocity component perpendicular to the surface. All factors considered, an upper limit on the error in the effective incidence velocity of the beam upon the grating surface is given by $\Delta v_{y,\max} \simeq 0.26$ m/s.

IV. INTERACTION POTENTIAL

Since quantum reflection of helium atoms occurs more than 10 nm above the surface, it is sufficient to use the (highly retarded) asymptotic form of the Casimir-Polder potential to describe the interaction between the atoms and an uncharged surface [18,36]. If, in addition, the voltage ϕ is applied between two neighboring grating bars (see inset in Fig. 1), an electric field $\mathbf{E}(x,y)$ is induced. The resulting electrostatic interaction potential [44] must be added to the Casimir-Polder interaction in order to yield the total potential for a polarizable particle at position (x,y) above the surface,

$$V(x,y) = -\frac{C_4(x)}{[y+\Omega(x)]^4} - \frac{\alpha}{2}|\mathbf{E}(x,y)|^2, \qquad (1)$$

with α the static polarizability. Here, $y + \Omega(x)$ approximates the closest distance between the particle and the surface as specified by the surface function $\Omega(x)$ with period L. In the present case we have $\Omega(x) = 0$ above the grating bars and $\Omega(x) = \Omega_0$ between them; see Fig. 1.

The function $C_4(x)$ accounts for the fact that the dielectric permittivity of the conductive grating bars differs from that of the dielectric between the bars. This modifies the C_4 parameter

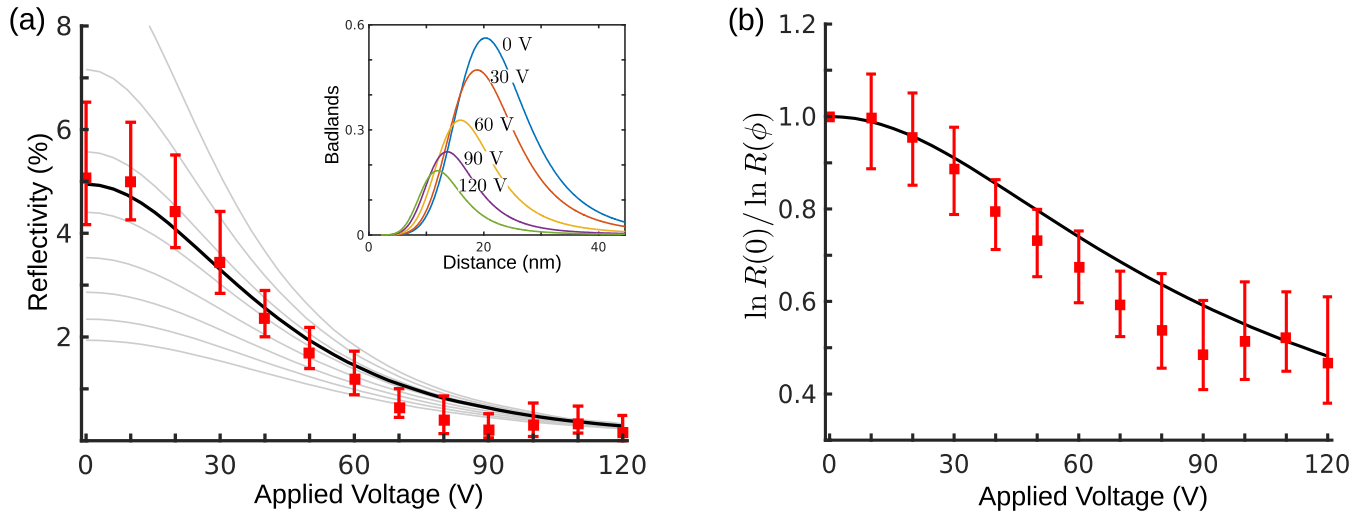

FIG. 2. (a) Measured specular reflectivity as a function of applied voltage (red squares) compared to simulations with impinging velocities ranging from 0.6 to 1.3 m/s (in 0.1 m/s steps; gray lines) and for 0.82 m/s (corresponding to $\theta = 1.35$ mrad for the mean velocity of the beam; black line). The inset shows the badlands function for different voltages, indicating the region contributing to quantum reflection. (b) Comparison between the experimental data (red squares) and the simple analytic model (5) (black line).

locally according to the relation [33]

$$C_4(x) = \frac{C_4}{2}\int_1^\infty \frac{d\xi}{\xi^4}\left[\frac{s(\xi,x)-\xi}{s(\xi,x)+\xi} + (1-2\xi^2)\frac{s(\xi,x)-\varepsilon_r(x)\xi}{s(\xi,x)+\varepsilon_r(x)\xi}\right], \tag{2}$$

with $C_4 = 3\hbar c\alpha/32\pi^2\varepsilon_0$, $s(\xi,x) = \sqrt{\varepsilon_r(x) - 1 + \xi^2}$; $\varepsilon_r(x)$ is the dielectric permittivity of the material at position x. In the present experiment we have $C_4(x) = C_4$ above the conductive grating bars ($\varepsilon_r \gg 1$), whereas one obtains $C_4(x) \equiv C_{4,\mathrm{Si}} \simeq 0.46 C_4$ above the silica surface ($\varepsilon_r \simeq 4$) between the grating bars.

Since the total potential (1) is periodic, only integer multiples of the grating momentum $2\pi\hbar/L$ can be transferred to the outgoing matter wave in grating direction x. Moreover, only specular reflection occurs in the present experiment. This is due to the high velocity parallel to the surface, $v \simeq 605$ m/s, in combination with the relatively small grating period, $L = 10$ μm, which implies a large change in normal kinetic energy even for scattering into the first diffraction order (see Appendix B). This allows us to restrict the theoretical consideration to the one-dimensional Schrödinger equation with the specular interaction potential

$$V_{\mathrm{sp}}(y) = -\frac{C_4}{2y^4} - \frac{C_{4,\mathrm{Si}}}{2(y+\Omega_0)^4} - \frac{\alpha}{2L}\int_0^L dx\,|\mathbf{E}(x,y)|^2, \tag{3}$$

obtained by averaging (1) in the x direction. The simplification is supported by numerical wave-packet simulations, which show that diffraction should only become observable at much lower parallel velocities.

V. QUANTUM REFLECTION

Figure 2 shows the reflection probability measured for bias voltages from 0 to 120 V (red squares) compared to the numerical simulations (solid lines). The signal is determined by subtracting the helium background and compensating for the partial overlap of the beam with the grating as well as for the finite width of the detection selector slit. The error bars are the standard deviation as obtained from multiple runs of the experiment and also take into account the error in the geometrical correction factor [43]. It clearly demonstrates that quantum reflection can be suppressed by controlling the electric field above the surface. The experimentally observed dependence on applied voltage ϕ is in good agreement with the numerical results.

In order to calculate the reflectivity, we solve the stationary Schrödinger equation with the specular interaction potential (3) by use of the log-derivative method [45]. The electric field $\mathbf{E}(x,y)$ is also computed numerically by solving Poisson's equation. [The total interaction potential (3) is illustrated in Appendix C.] Since the Casimir-Polder potential dominates over the electrostatic interaction close to the surface, one can express boundary conditions for the matter waves as $y \to 0$ in terms of outgoing WKB waves solely determined by the Casimir-Polder potential [39]. The reflectivities depend strongly on the velocity towards the surface. Since the latter is not exactly known, we solve the Schrödinger equation for incident velocities ranging from 0.6 to 1.3 m/s in steps of 0.1 m/s [gray lines in Fig. 2(a)]. Assuming an incidence velocity $v_y \simeq 0.82$ m/s (corresponding to an angle $\theta = 1.35$ mrad for the mean velocity of the beam) yields excellent agreement between the experimental data and the simulations and is reasonably within the experimental uncertainty [black solid line in Fig. 2(a)].

The inset in Fig. 2(a) shows the badlands as a function of distance y from the surface for different applied voltages. This function indicates which regions contribute to quantum reflection and it is given by $B(y) = \hbar^2|3p'^2(y) - 2p(y)p''(y)|/4p^4(y)$ [36] with $p^2(y) = m^2v_y^2 - 2mV_{\mathrm{sp}}(y)$. The badlands clearly decrease with increasing bias.

VI. QUALITATIVE DESCRIPTION

In order to approximately understand the bias-induced reflectivity reduction, we consider a simplified scenario where

the height Ω_0 of the electrodes is negligible, and thus the potential at the surface $y = 0$ can be described by the smooth function $\phi_{\rm surf}(x)$. Then, to leading order $\phi_{\rm surf}(x) \simeq \phi \sin(\pi x/L)/2$ (see Appendix C). The resulting electrostatic potential is $\phi(x,y) = \phi \sin(\pi x/L) \exp(-\pi y/L)/2$, which approaches asymptotically the numerical solution of the Poisson equation as $y/L \to \infty$. Hence, the total interaction potential is to leading order independent of x and decays exponentially with the distance from the surface,

$$V_{\rm eff}(y) = -\frac{C_4}{y^4} - \frac{\alpha}{2}\left(\frac{\phi\pi}{2L}\right)^2 e^{-2\pi y/L}. \tag{4}$$

We remark that above-barrier reflection of the combined attractive Casimir-Polder and a *repulsive* exponential potential induced by a blue-detuned evanescent wave atomic mirror was theoretically studied in Refs. [46–48].

In the current experiment, field-free quantum reflection of helium atoms occurs roughly at $y \simeq 20$ nm above the unbiased metallic surface ($2\pi y/L \simeq 10^{-2}$); see inset in Fig. 2(a). Since the electrostatic interaction shifts the badlands even closer to the surface, the particle has effectively gained the energy $\alpha\phi^2\pi^2/8L^2$ when entering the badlands. Given that for small $v \sin\theta$ the probability of quantum reflection depends exponentially on the impact velocity $v \sin\theta$ [36], one obtains for the bias-dependent reflectivity $R(\phi)$,

$$\frac{\ln R(\phi)}{\ln R(0)} = \sqrt{1 + \frac{\alpha}{m}\left(\frac{\pi\phi}{2Lv\sin\theta}\right)^2}. \tag{5}$$

Thus, the electrostatic interaction potential increases the velocity of the impinging matter wave and therefore decreases its reflectivity, in accordance with experimental and numerical findings. In Fig. 2(b) we show the experimental reflectivities together with the estimate of Eq. (5). While relation (5) cannot be used to predict the exact dependence of the reflectivity on the applied voltage it nevertheless allows one to estimate and understand the controlled suppression of quantum reflection with increasing bias ϕ.

VII. CONCLUSIONS

We demonstrated that an electric field can be used to accurately control quantum reflection. The good agreement between experiment and theory opens the door to the design of tunable quantum reflection devices. For instance, manufacturing a two-dimensional array of electric gratings realizes a switchable diffraction grating. Such a grating will show specular reflection for zero bias while the matter wave gets diffracted if its reflection is locally suppressed by an applied voltage [39]. In a similar fashion, one might think of designing other reflective optical elements, such as Fresnel mirrors [49], which can be used for tunable reflective focusing of matter waves.

Relation (5) indicates that an electric switch for quantum reflection should work equally well for clusters of arbitrary size because the bias-dependent suppression of reflectivity depends only on the ratio between polarizability and mass, α/m, and is thus approximately independent of the cluster size. In contrast, the dependence on the ratio α/m might be a viable tool to separate different molecular species of the same velocity.

ACKNOWLEDGMENT

We thank T. Nitschke for helpful discussions.

APPENDIX A: DETECTION SCHEME

Detection of the neutral helium beam was achieved by electron-impact ionization and time-of-flight mass spectrometry. For ionization, a custom radial electron-impact ionizer was used. The ionizer consists of multiple components designed for optimizing and shaping of the space-charge-limited, low-energy electron cloud, yielding a relatively strong signal with only a short ionization pulse, thus also reducing detection of the background. A detailed view is presented in Ref. [43].

Following ionization the helium ions enter a Wiley-McLaren-type time-of-flight mass spectrometer operated at 2 kV and then continued to be detected by an Even-cup detection assembly, which consists of a 9-kV negatively biased electrode housing a gold-plated polished glass disk, and a negatively biased channel electron multiplier. The helium ions are accelerated towards the electrode and through the biased grid and emit secondary electrons upon impact with the gold layer. The emitted electrons are pushed away from the electrode to be collected by the channel electron multiplier, which is connected to an amplifier that feeds an oscilloscope which registers the signal and transmits it to a PC to be analyzed. The described scheme yields extremely high detection efficiency.

APPENDIX B: QUANTUM REFLECTION FOR LARGE TANGENTIAL VELOCITIES

We consider quantum reflection of an impinging matter wave in grazing incidence at angle $\theta \ll 1$ with wave numbers $k_x = mv/\hbar$ and $k_y \simeq mv\theta/\hbar$ parallel and perpendicular to the surface, respectively. In order to calculate the reflection probabilities into the different diffraction orders, one has to solve the stationary Schrödinger equation for the wave function $\varphi(x,y)$. Exploiting the periodicity along the grating direction x leads to the ansatz [39,50]

$$\varphi(x,y) = e^{ik_x x} \sum_{n\in\mathbb{Z}} \varphi_n(y) e^{ik_n y} e^{i2\pi n x/L}. \tag{B1}$$

The wave number k_n perpendicular to the surface is for each diffraction order n determined by the conservation of energy,

$$k_n^2 = k_x^2 + k_y^2 - \left(k_x + \frac{2\pi n}{L}\right)^2. \tag{B2}$$

In the present case, this can be further simplified to $k_n^2 \simeq k_y^2 - 4\pi n k_x/L$ since $2\pi/Lk_y \simeq 10^{-2}$. This implies that only negative diffraction orders $n \leqslant 0$ are open, $k_n^2 > 0$, while positive diffraction order are closed, $k_n^2 < 0$. In addition, even for $n = -1$, the transferred normal kinetic energy is relatively large: $k_{-1}^2/k_y^2 \simeq 33$.

To see how this situation leads only to specular reflection, we consider the stationary Schrödinger equation in the comoving frame, i.e., for $\psi(x,y) = e^{-ik_x x}\varphi(x,y)$

$$\left(\partial_x^2 + 2ik_x\partial_x + \partial_y^2 + k_y^2\right)\psi(x,y) - \frac{2m}{\hbar^2}V(x,y)\psi(x,y) = 0. \tag{B3}$$

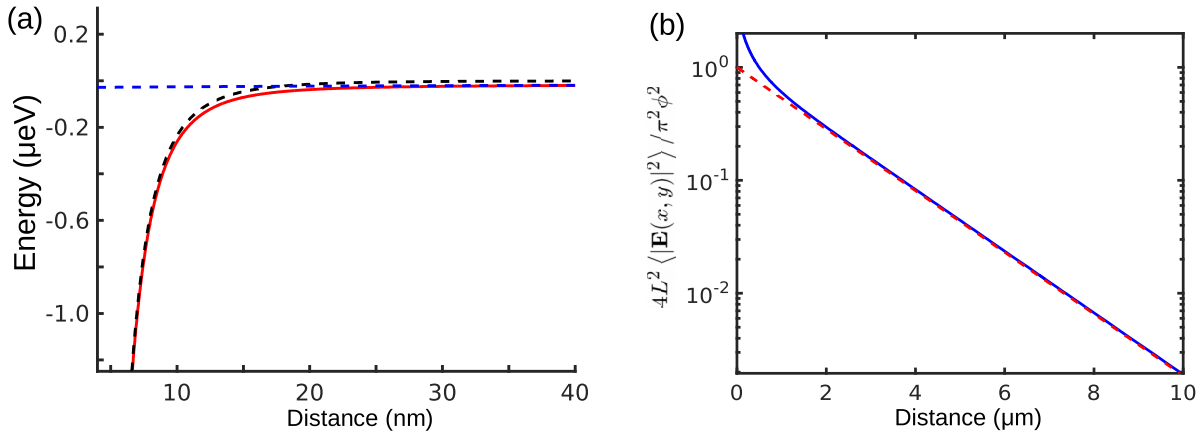

FIG. 3. (a) Specular interaction potential (3) at $\phi = 60$ V as function of distance from the grating (solid red line), together with the pure electrostatic interaction (dashed blue line) and the pure Casimir-Polder interaction (dashed black line). (b) Squared modulus of the electric field averaged over one grating period: exact numerical solution (solid blue line) compared to the approximate solution (C3) (dashed red line).

Since $\partial_x\psi(x,y) \propto 2\pi/L$ according to Eq. (B1) and since $2\pi k_x/Lk_y^2 \gg 1$, it follows that $\psi(x,y) \simeq \varphi_0(y)$ because otherwise Eq. (B3) would include divergent contributions. Spatially averaging over one grating period then results in the stationary Schrödinger equation

$$\left(\partial_y^2 + k_y^2\right)\varphi_0(y) - \frac{2m}{\hbar^2}V_{\rm sp}(y)\varphi_0(y) = 0, \tag{B4}$$

with the specular interaction potential

$$V_{\rm sp}(y) = \frac{1}{L}\int_0^L dx\, V(x,y). \tag{B5}$$

In Fig. 3(a) we show the specular interaction potential (3) as obtained from the exact solution of the electrostatic problem. The figure demonstrates that the electrostatic interaction is constant in the region where quantum reflection takes place and that it reduces the reflection probability off the Casimir-Polder potential by increasing the particle impact velocity. For distances large compared to the Casimir-Polder length scale the electrostatic interaction potential dominates the total interaction potential.

APPENDIX C: ASYMPTOTIC FORM OF THE ELECTRIC FIELD

In order to calculate the squared modulus of the electric field, $|\mathbf{E}(x,y)|^2$, we solve numerically the Poisson equation for the electrostatic potential $\Phi(x,y)$ with the boundary conditions as specified in the inset of Fig. 1 of the main text. The asymptotic behavior of the field, however, can be obtained by neglecting the details of the surface structure and solving the Laplace equation for $y > 0$,

$$\left(\partial_x^2 + \partial_y^2\right)\Phi(x,y) = 0, \tag{C1}$$

with the boundary condition $\Phi(x,0) = \phi_{\rm surf}(x)$. Due to the symmetry of the grating, it is sufficient to solve Eq. (C1) for $0 \leqslant x \leqslant L$ and use that $\Phi(0,y) = \Phi(L,y) = 0$. (The biased electrode at potential $\pm\phi/2$ is positioned at $L/4 \leqslant x \leqslant 3L/4$.) Thus, the electrostatic field can be expanded in a Fourier series,

$$\Phi(x,y) = \sum_{n=1}^{\infty}\Phi_n \sin\left(\frac{n\pi x}{L}\right)\exp\left(-\frac{n\pi y}{L}\right), \tag{C2}$$

where the coefficients Φ_n are the Fourier coefficients of the surface potential $\phi_{\rm surf}(x)$. For large distances, $\pi y/L \gg 1$, the electrostatic potential (C2) decays exponentially and the surface potential oscillates approximately between $\pm\phi/2$ and zero: $\phi_{\rm surf}(x) \simeq \pm\phi\sin(\pi x/L)/2$. Thus, the squared modulus of the electric field is for large distances well approximated by

$$|\mathbf{E}(x,y)|^2 \simeq \left(\frac{\phi\pi}{2L}\right)^2 e^{-2\pi y/L}. \tag{C3}$$

This asymptotic form agrees with the exact numerical solution of the Poisson equation, including the surface structure and the dielectric, averaged over one grating period L; see Fig. 3(b).

[1] L. D. Landau and E. Lifshitz, *Course of Theoretical Physics, Vol 3: Quantum Mechanics* (Pergamon Press, London, 1958).
[2] W. Brenig, Z. Phys. B **36**, 227 (1980).
[3] J. Böheim, W. Brenig, and J. Stutzki, Z. Phys. B **48**, 43 (1982).
[4] V. U. Nayak, D. O. Edwards, and N. Masuhara, Phys. Rev. Lett. **50**, 990 (1983).
[5] D. P. Clougherty and W. Kohn, Phys. Rev. B **46**, 4921 (1992).
[6] J. J. Berkhout, O. J. Luiten, I. D. Setija, T. W. Hijmans, T. Mizusaki, and J. T. M. Walraven, Phys. Rev. Lett. **63**, 1689 (1989).
[7] J. M. Doyle, J. C. Sandberg, I. A. Yu, C. L. Cesar, D. Kleppner, and T. J. Greytak, Phys. Rev. Lett. **67**, 603 (1991).
[8] I. A. Yu, J. M. Doyle, J. C. Sandberg, C. L. Cesar, D. Kleppner, and T. J. Greytak, Phys. Rev. Lett. **71**, 1589 (1993).
[9] F. Shimizu, Phys. Rev. Lett. **86**, 987 (2001).
[10] F. Shimizu and J.-i. Fujita, Phys. Rev. Lett. **88**, 123201 (2002).
[11] H. Oberst, D. Kouznetsov, K. Shimizu, J.-i. Fujita, and F. Shimizu, Phys. Rev. Lett. **94**, 013203 (2005).
[12] V. Druzhinina and M. DeKieviet, Phys. Rev. Lett. **91**, 193202 (2003).

[13] B. S. Zhao, H. C. Schewe, G. Meijer, and W. Schöllkopf, Phys. Rev. Lett. **105**, 133203 (2010).
[14] T. A. Pasquini, Y. Shin, C. Sanner, M. Saba, A. Schirotzek, D. E. Pritchard, and W. Ketterle, Phys. Rev. Lett. **93**, 223201 (2004).
[15] T. A. Pasquini, M. Saba, G.-B. Jo, Y. Shin, W. Ketterle, D. E. Pritchard, T. A. Savas, and N. Mulders, Phys. Rev. Lett. **97**, 093201 (2006).
[16] A. L. Marchant, T. P. Billam, M. M. H. Yu, A. Rakonjac, J. L. Helm, J. Polo, C. Weiss, S. A. Gardiner, and S. L. Cornish, Phys. Rev. A **93**, 021604(R) (2016).
[17] B. S. Zhao, S. A. Schulz, S. A. Meek, G. Meijer, and W. Schöllkopf, Phys. Rev. A **78**, 010902 (2008).
[18] B. S. Zhao, G. Meijer, and W. Schöllkopf, Science **331**, 892 (2011).
[19] B. S. Zhao, W. Zhang, and W. Schöllkopf, Mol. Phys. **111**, 1772 (2013).
[20] B. S. Zhao, W. Zhang, and W. Schöllkopf, Sci. Adv. **2**, e1500901 (2016).
[21] A. D. Cronin, J. Schmiedmayer, and D. E. Pritchard, Rev. Mod. Phys. **81**, 1051 (2009).
[22] K. Hornberger, S. Gerlich, P. Haslinger, S. Nimmrichter, and M. Arndt, Rev. Mod. Phys. **84**, 157 (2012).
[23] T. Juffmann, H. Ulbricht, and M. Arndt, Rep. Prog. Phys. **76**, 086402 (2013).
[24] T. Reisinger, A. A. Patel, H. Reingruber, K. Fladischer, W. E. Ernst, G. Bracco, H. I. Smith, and B. Holst, Phys. Rev. A **79**, 053823 (2009).
[25] T. Reisinger, G. Bracco, and B. Holst, New J. Phys. **13**, 065016 (2011).
[26] D. Kouznetsov and H. Oberst, Phys. Rev. A **72**, 013617 (2005).
[27] D. Kouznetsov, H. Oberst, A. Neumann, Y. Kuznetsova, K. Shimizu, J.-F. Bisson, K. Ueda, and S. R. J. Brueck, J. Phys. B **39**, 1605 (2006).
[28] T. Reisinger, S. Eder, M. M. Greve, H. I. Smith, and B. Holst, Microelectron. Eng. **87**, 1011 (2010).
[29] S. Eder, T. Reisinger, M. Greve, G. Bracco, and B. Holst, New J. Phys. **14**, 073014 (2012).
[30] R. E. Grisenti, W. Schöllkopf, J. P. Toennies, G. C. Hegerfeldt, and T. Köhler, Phys. Rev. Lett. **83**, 1755 (1999).
[31] S. Y. Buhmann, S. Scheel, S. A. Ellingsen, K. Hornberger, and A. Jacob, Phys. Rev. A **85**, 042513 (2012).
[32] H. B. G. Casimir and D. Polder, Phys. Rev. **73**, 360 (1948).
[33] S. Y. Buhmann, *Dipsersion Forces I: Macroscopic Quantum Electrodynamics and Ground-State Casimir, Casimir-Polder and van der Waals Forces* (Springer, Berlin, 2012).
[34] R. Côté, H. Friedrich, and J. Trost, Phys. Rev. A **56**, 1781 (1997).
[35] C. Eltschka, M. J. Moritz, and H. Friedrich, J. Phys. B **33**, 4033 (2000).
[36] H. Friedrich and J. Trost, Phys. Rep. **397**, 359 (2004).
[37] G. Dufour, R. Gurout, A. Lambrecht, and S. Reynaud, Europhys. Lett. **110**, 30007 (2015).
[38] G. Dufour, R. Gurout, A. Lambrecht, and S. Reynaud, J. Phys. B **48**, 155002 (2015).
[39] B. A. Stickler, U. Even, and K. Hornberger, Phys. Rev. A **91**, 013614 (2015).
[40] U. Even, EPJ Tech. Instrum. **2**, 1 (2015).
[41] U. Even and B. Dick, Rev. Sci. Instrum. **71**, 4415 (2000).
[42] H. Haberland, *Clusters of Atoms and Molecules: Theory, Experiment, and Clusters of Atoms*, Vol. 52 (Springer Science & Business Media, New York, 2013).
[43] See Supplemental Material at http://link.aps.org/supplemental/10.1103/PhysRevA.95.043639 for a description of alignment procedure, data analysis, and electron-impact ionizer.
[44] J. D. Jackson, *Classical Electrodynamics* (Wiley, New York, 1999).
[45] B. Johnson, J. Comput. Phys. **13**, 445 (1973).
[46] B. Segev, R. Côté, and M. G. Raizen, Phys. Rev. A **56**, R3350 (1997).
[47] R. Côté, B. Segev, and M. G. Raizen, Phys. Rev. A **58**, 3999 (1998).
[48] R. Côté and B. Segev, Phys. Rev. A **67**, 041604 (2003).
[49] T. E. Judd, R. G. Scott, G. Sinuco, T. W. A. Montgomery, A. M. Martin, P. Krüger, and T. M. Fromhold, New J. Phys. **12**, 063033 (2010).
[50] S. Miret-Artés and E. Pollak, J. Phys. Chem. Lett. **8**, 1009 (2017).